2014 IEEE International Conference on Robotics & Automation (ICRA)
Hong Kong Convention and Exhibition Center
May 31 - June 7, 2014. Hong Kong, China

Estimation of Tissue Stiffness using a Prototype of Air-float Stiffness Probe

Indika B. Wanninayake, Lakmal D. Seneviratne, *Member, IEEE,* and Kaspar Althoefer, *Member, IEEE*

***Abstract*— This paper presents a novel technique for estimating stiffness distribution of a soft tissue using a prototype of air-float stiffness probe. The air-float stiffness probe uses an indentation technique to estimate tissue stiffness. It consists of a spherical indenter and an indentation depth sensing mechanism that operates under a supply of compressed air. The probe has the ability to estimate tissue stiffness in non-planner tissue profiles. A novel technique to estimate indentation force, using supply air pressure is described and validated using both experimental procedures and finite element analysis (FEA) techniques. FEA package, ANSYS CFX was used for analyzing in 2D the solid-fluid interactions within the probe to estimate force available at the indenter at different supply air pressure settings. Both the experimental results and numerical simulations suggest that there is a very strong linear correlation between the indentation force and the supply air pressure. This relationship is used to estimate the indentation force in real time during an indentation test. Verification tests carried out on simulated silicon samples showed that the probe is capable of estimating tissue stiffness values with high accuracy and repeatability.**

I. Introduction

The change in stiffness is recognized as one of the most important parameters in differentiating malignant tumors from healthy tissues as many pathological changes are associated with stiffness change. According to Krouskop *et al* [1], stiffness of tumors can be up to several times higher than the stiffness of surrounding healthy tissues. In an open surgery with direct access to the surgical field, the surgeon has the option to palpate organs to identify and locate tumors. However, in advanced surgical techniques such as minimally invasive surgery (MIS), due to lack of tactile and force feedback, surgeons have to rely on other techniques for soft tissues characterization. A number of attempts to develop tactile and force sensors for MIS, to assess soft tissue characteristics have been reported in the literature [2]-[11].

The work described in this paper was funded by the European Commission's Seventh Framework Programme under grant agreement 287728 in the framework of EU project STIFF-FLOP.

I.B. Wanninayake is with King's College London, Department of Informatics, The Strand, London, U.K. WC2R 2LS and also with Kingston University London, SW15 3DW, London, U.K. (e-mail: w.wanninayake@kingston.ac.uk)

L.D. Seneviratne is with King's College London, Department of Informatics, The Strand, London, U.K., WC2R 2LS, (e-maill: lakmal.seneviratne@kcl.ac.uk), and also with the College of Engineering, Khalifa University of Science, Technology and Research, Abu Dhabi, U.A.E. (e-mail: lakmal.seneviratne@kustar.ac.ae).

K. Althoefer is with King's College London, Department of Informatics, The Strand, London, U.K. WC2R 2LS L, (e-mail: k.althoefer@kcl.ac.uk).

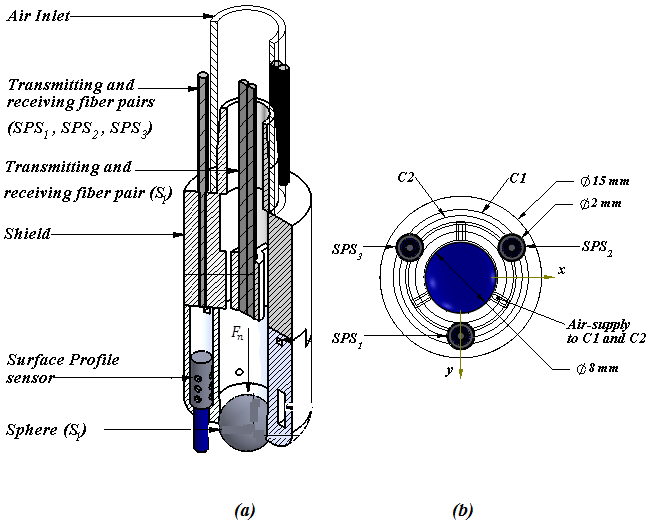

Fig. 1. (a) Longitudinal section of the air-float palpation probe indicating the location of fiber optic displacement sensors, $SPSs, and\ S_1$, (b) Top view of the stiffness probe indicating probe dimensions.

Uribe *et al.* [2] have developed a piezoelectric bimorph to extract soft tissue characteristics. The system operates on an AC voltage supply and once supplied bimorph at near resonant frequency. When in contact with the tissue, the shift in frequency and the amplitude is used to differentiate various tissue properties. In [9], a finger like probe with tactile sensors made out of piezoelectric polymer films is used to characterize tissue properties. The tactile sensor reported in [10] can predict the stiffness of the object in contact irrespective of the geometry and the thickness of the object.

In [11] Ottensmeyer *et al.* use an indentation technique, a 12mm cannula with an indenter to acquire visco-elastic properties of soft tissues. Here, the force and indentation depth relationship is evaluated using a force sensor and a LVDT (Linear Variable Differential Transformer) position sensor. However, the LVDT used here measure only the extension of the indenter and not the actual indentation depth. Hence the accuracy of the stiffness calculation cannot be guaranteed unless the probe is held normal to the tissue surface at a predefined distance. In order to use an indentation technique to evaluate elastic modulus of a tissue, it is essential that both absolute indentation depth and the component of the tissue reaction force, which is the force normal to the tissue surface, are measured. Here, the absolute indentation depth is the distance measured from the tip of the indenter to the tissue surface along the normal.

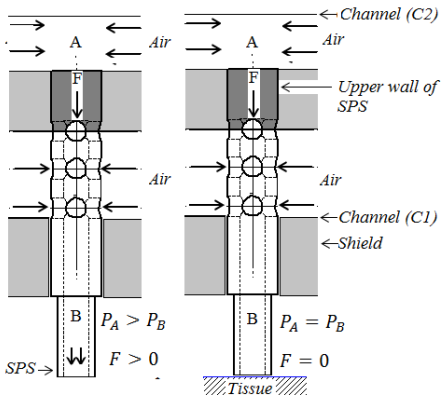

Fig. 2. Behavior of the surface profile sensors ($SPSs$) and forces acting on the upper wall of the.

One of most commonly used method to estimate absolute indentation depth is by using a depth-sensing camera that assesses the local deformability of the tissue. According to Johnson et al. [12], due to the high local deformability of soft tissues, indentation contours rise to the tissue surface following an exponential curve. Tactile sensors reported in [13]-[15] use information obtained through a structured-light camera and a force sensor to assess elasticity parameters of deformable objects. However, the main disadvantage of this technique is that the manipulator used to deform the tissue may occlude the parts of the deformed objects limiting accuracy of the output. In [18], Liu et al. suggest a new approach to identify tissue surface profile variations. This system uses four optical-fiber displacement-sensing elements, each with a cylindrical rod that slides over the tissue surface to track the tissue deformation. Although this method can estimate indentation depth in real time, the sliding rods are designed to be extended outward by gravity, hence the system works only when the tool is held vertically. In view of the limitations associated with the above-mentioned techniques, a new approach for estimating tissue elastic properties is proposed in this paper. Initial research leading to the design of this probe was presented in [16]. Work described in this paper extends the capability of the probe further by incorporating stiffness computations to aid tissue characterization. A number of tests have been carried out using simulated soft tissues to evaluate and verify the ability of the probe to estimate tissue stiffness accurately.

II. Development of the Air-Float Stiffness Probe

A. Design of the probe

As illustrated in Fig. 1, the air-float stiffness probe has a hollow cylindrical body with one of its ends connected to a pressurized air supply. At the tip of the probe there are four displacement sensing elements, a spherical indenter (S_1) at the center and three surface profile sensors ($SPSs - SPS_1, SPS_2$ and SPS_3) arranged in a circle at 120° each other surrounding the indenter. Displacement of each sensing element is measured optically using a pair of optical fibers above each sensing element. The indenter S_1 is free to rotate while all the four sensing elements can move axially, parallel to the probe axis. These sensing elements are mounted inside the probe in such a way that, during an indentation test as the probe moves over the tissue, the indenter S_1 indents the tissue and roll over it while the three $SPSs$ follow the tissue curvature. The two circular channels towards the tip of the probe $(C1, C2)$ delivers air to $SPSs$. The three $SPSs$ are designed and mounted within the probe in such a way that they can deliver and discharge air out at the tip. As illustrated in Fig. 2, when the probe is pressurized, the differential pressure on the upper wall of each SPS move it outward until a contact is made. Once the contact is established, air-cushion at the tip of SPS keeps it floating just above the tissue surface. This ensures continuous tracking of the tissue surface. The three $SPSs$ generates a datum line for the measurements made by S_1 to calculate the absolute indentation depth. The prototype was built using a 3D rapid prototyping machine (ProJetTM HD 3000 Plus), which has a minimum layer resolution of 16μm. Digital fiber optic amplifier FS-N10MN, Keyence Corporation is used in the optical detection circuit. Calibration results for the four displacement sensors are given in Fig. 3.

B. Indentation depth estimation

As illustrated in Fig. 4, the indentation depth measuring system is defined in the Cartesian coordinate system with the origin 'O' at the center of the probe face. The x-y plane is chosen to coincide with the end face of the probe while z-axis is coinciding with the central axis of the probe. The radius of the indenter S_1 is r. As the S_1 indents the tissue sample, three $SPSs$ follow the tissue profile around the S_1 to generate plane $D_1D_2D_3$, approximating the tissue profile underneath the probe.

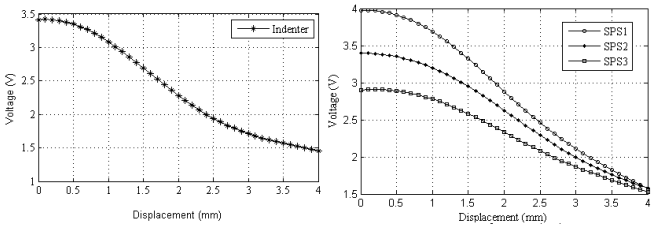

(a) (b)

Fig. 3. Calibration results for (a) the indenter (S_1) and (b) the three surface profile sensors (SPS_1, SPS_2, SPS_3)

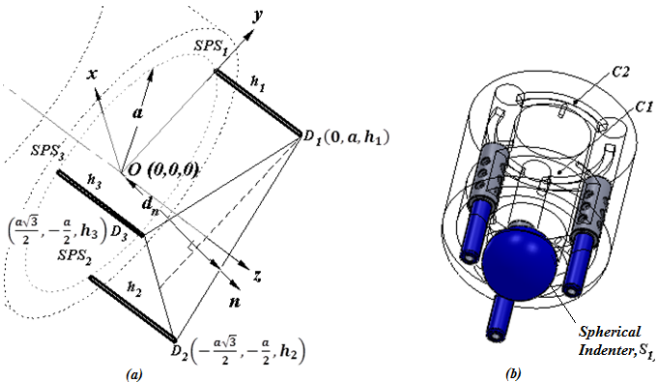

Fig. 4. Modeling the indentation depth and the orientation of the probe with respect to the tissue surface, coordinates of the three surface profile sensor tips are $D_3(0, a, h_1)$, $D_2\left(-\frac{a\sqrt{3}}{2}, -\frac{a}{2}, h_2\right)$ and $D_1\left(\frac{a\sqrt{3}}{2}, -\frac{a}{2}, h_3\right)$.

Then, the normal distance from the deepest indentation point of S_1 to the plane $D_1D_2D_3$, can be used to establish an equation for absolute indentation depth d_{in} and that is

$$d_{in} = r - d_n - (r - h_4)\cos\theta_z. \quad (1)$$

Here, d_n is the normal distance from the probe face to the tissue plane and can be written as

$$d_n = \frac{a(h_1+h_2+h_3)}{\sqrt{2((h_2-h_1)^2+(h_3-h_1)^2+(h_3-h_2)^2)+9a^2)}}. \quad (2)$$

The angle θ_z can be written as,

$$\theta_z = \cos^{-1}\left(\frac{3a}{\sqrt{2((h_2-h_1)^2+(h_3-h_1)^2+(h_3-h_2)^2)+9a^2)}}\right). \quad (3)$$

Here, h_1, h_2, h_3 and h_4 are the extensions of each SPSs (SPS_1, SPS_2 and SPS_3) and S_1 from the face of the probe. The full derivation of (1), (2) and (3) is given in [16].

III. Estimating Indentation Force from Supply Air Pressure

A. Computational model: Fluid force acting on the indenter

A two dimensional (2D) axisymmetric computational model was developed to simulate the behavior of the air-float probe and to establish a relationship between indentation force and the supply air pressure. ANSYS CFX, a commercial computation fluid dynamic (CFD) package was used for this study. The size of the computational domain, physical arrangement, mesh, and the boundary conditions are illustrated in Fig. 5. Inner wall diameter of the probe was 8mm and simulations were done for two different indenter sizes (7mm and 7.6mm diameter) to evaluate fluid force acting on the indenter under different wall clearance values. In order to simplify the computational model, it was assumed that the flow at the inlet of the probe is laminar with turbulence intensity below 5%. Further, aerodynamic forces induced due to the rotation of the spherical indenter is ignored and it was assumed that there is no swirl in the flow. A series of simulations were carried out for six different indenter positions along the probe axis and at each position, the same simulation was repeated for at least three inlet velocity settings (from 1m/s to 7m/s). Three user define functions were used to compute force on the indenter and the area weighted average of pressure at the inlet and at the indenter.

Fig. 6 shows the variation of the force on the spherical indenter for different inlet pressure values. It is quite clear from this simulation result that the relationship between the pressure and indentation force is linear. As we modify the clearance between the indenter and probe inner wall, gradient of the force-inlet pressure curve changes, however linear relationship remains. Although this is a non-linear relationship, indentation force follows the pressure variation inside the probe (see Fig. 7). Hence the indentation force at any point can be predicted given that air pressure at the inlet is known.

Geometry Boundary	Boundary Type
Inlet	Velocity Inlet
Opening	Pressure outlet (0 Pa)
Outlet	Pressure outlet (0 Pa)
Probe wall	wall
Probe axis	Symmetry
Tissue	wall
Sphere	wall

(a)

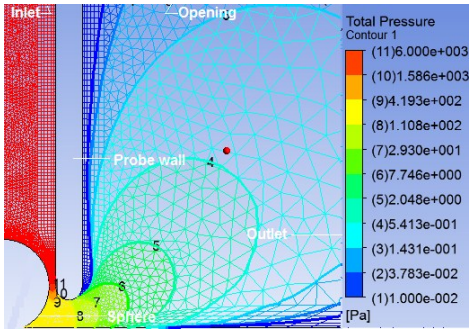

(b)

Fig. 5. (a). Schematic of the computational domain and the pressure distribution of the probe at inlet speed 1m/s. Boundary conditions are given in (b), Domain size (width=500mm, height = 100mm)

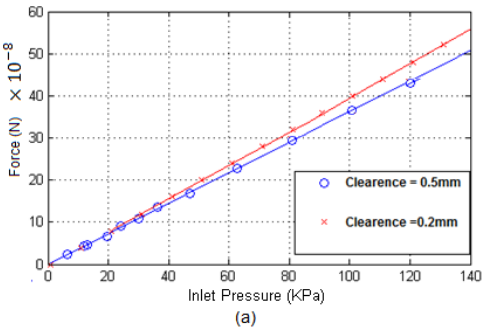

(a)

Fig. 6. Relationship between Inlet air pressure and force (on 2D spherical element), RMSE (root-mean-square error) for 0.5mm and 0.2mm clearance values were 0.29 and 0.23 respectively

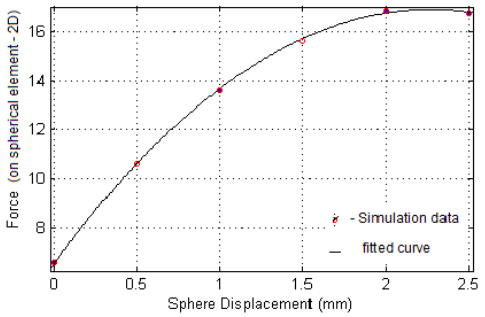

Fig. 7. Relationship between Indentation force and the displacement of the indenter.

B. *Experimental Verification*

The relationship predicted above, between indentation force (F_n) and inlet air pressure (P_s), was validated using an experimental procedure. In this, the probe was pressed against a ATI Mini 40 force sensor rigidly mounted to a workbench. The air-float probe was attached to a robotic manipulator for accurate motion control and the probe was connected to a compressed air supply. The supply air pressure was adjusted to 30KPa using an electrically controlled pressure regulator. The experimental setup is shown in Fig. 8. During calibration; the robot arm was slowly advanced towards and retrieved from the Mini40. As the probe moves, force information from the ATI Mini 40 and air pressure oscillations from the pressure sensor integrated to the pressure regulator were collected using a DAQ (data acquisition) card NI PCI 6013 and DAQ module USB6211 respectively. Experiment was repeated for ten advancing and retrieval cycles to evaluate the repeatability of data.

Fig. 9 shows the variation of force (F_n) and pressure inside the probe (P_s) with respect to the indenter displacement. The combined F_n-P_s relationship is shown in Fig. 10. It is clear from Fig. 10 that there is a linear correlation between the supply air pressure and the indentation force (see (4)). Although there is some hysteresis between the advancing and retrieving cycles in both P_s and F_n curves, the linear relationship predicts the indentation force with an RMSE less than 0.0404.

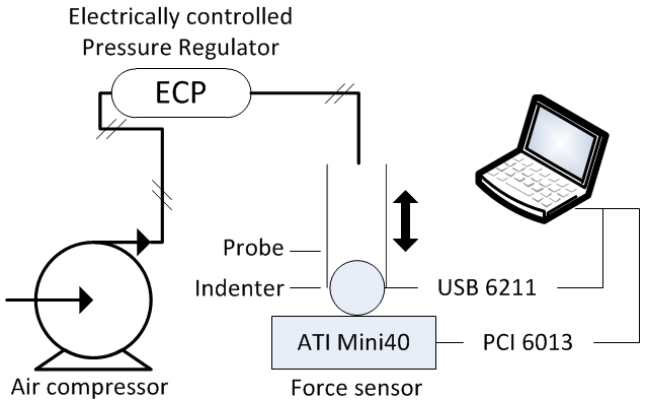

Fig. 8. Schematic of the experimental setup.

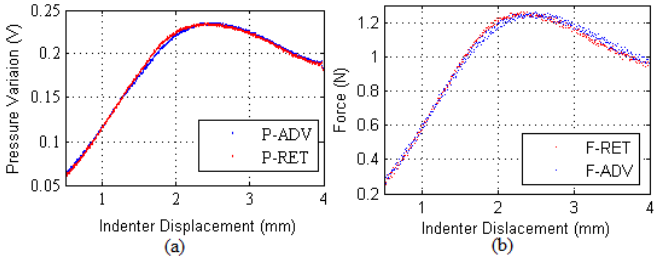

Fig. 9. Relationship between (a). Inlet air pressure and (b). Indentation force with respect to the displacement of the indenter, Pressure and force variation during advance and retrieval are marked as P-ADV, P-RET, F-ADV and F-RET respectively.

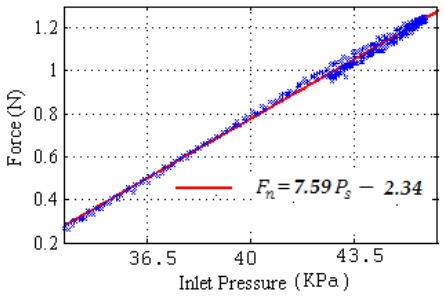

Fig. 10. Relationship between indentation force and inlet air pressure. The blue dots represent the experimental data, while the red solid line represents the fitted curve.

$$F_n = 7.59P_s - 2.34 \tag{4}$$

IV. Estimating Stiffness from the Indentation Force and Indentation Depth

The nature of the stress-strain relationship for any indentation test depends on number of factors including the shape and size of the indenter and viscoelastic properties of the material under investigation. For spherical indenters, this relationship is nonlinear as the contact area changes with the indentation depth. According to [17], the change in contact area (t) with the indentation depth can be estimated using

$$t = \sqrt{r d_{in}}\,. \tag{5}$$

Non-linearity is significant in materials such as soft tissue due to their high water content. However, at lower indentation depths, this relationship can successfully be approximated by a linear elastic model [18]. The choice of the linear elastic model depends mainly on the thickness and geometry of the tissue sample. A model such as Hertzian contact equation (see (6)) [18],

$$E = \frac{6F_r(1-v^2)}{8d_{in}\sqrt{rd_{in}}}, \tag{6}$$

can accurately represent stress-strain relationship if thickness of the tissue sample is large compared to the diameter of the indenter [21]. Here, E and v are the Young's modulus and the Poisson ratio of the tissue sample respectively. For incompressible materials such as soft tissues, v could be approximated to 0.5 [20]. However, to estimate stiffness of tissue samples with lower thickness (d)-radius ratios ($^{d}/_{r}$ < 10), an elastic model corrected for tissue sample thickness (see (7)) should be used to estimate tissue elasticity accurately [21].

$$E = \frac{6F_r(1-v^2)}{8d_{in}\sqrt{rd_{in}}(1+1.133\chi+1.283\chi^2+0.769\chi^3+0.0975\chi^4)}. \tag{7}$$

here,

$$\chi = \frac{\sqrt{rd_{in}}}{d}.$$

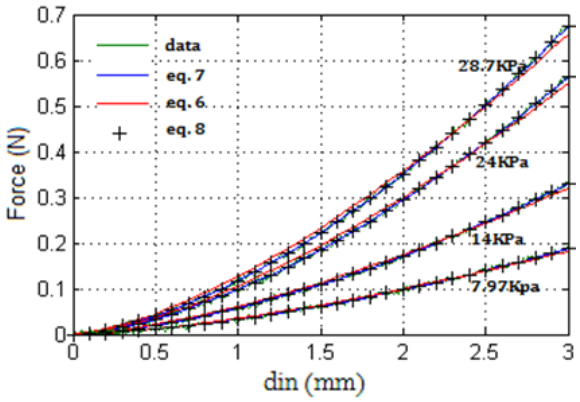

(a)

Test Location		Estimated Stiffness (KPa)		
		eq.(6)	eq.(7)	eq.(8)
26.4KPa	1	35	28.7	29.5
Sample	2	29.7	24	24.7
10.8KPa	1	9.88	7.97	8.2
sample	2	17.4	14	14.4

(b)

Fig. 11. (a). Tissue reaction force against the indentation depth for two test locations in each of 28KPa and 10.8KPa tissue samples.(b). Estimated elastic module for each of the test location estimated using (7), (8) and (9).

All the validation experiments presented in this paper were carried out with simulated tissue sample with lower $^{d}/_{r}$ ratios. Hence the stiffness of each sample was estimated using (7). However, for verification purposes, experimental data was tested against a commonly used nonlinear elastic model (Fung model (8)). As suggested by Lin et al [17], this model can be used to provide best fits of data for both biological tissues and synthetic gels.

$$F = \frac{20E\pi}{9\pi(1-\nu^2)}\left(\frac{t^5-15rt^4+75r^2t^3}{5rt^2-50r^2t+125r^3}\right)\exp\left[b\left(\frac{t^3-15rt^2}{25r^2t-125r^3}\right)\right] \quad (8)$$

To investigate the applicability of the above contact equations to model the air-float palpation probe, a series of indentation tests were carried out on two simulated silicon tissue samples made from RTV6166 gel. Stiffness of each of the sample was 26.4±4KPa and 10.8±2.8KPa. During the experiment the air-float probe was positioned onto each silicone phantom leaving a clearance of 1mm between the probe face and the tissue surface. Then the supply air pressure was increased from zero at a constant rate using the electrically controlled pressure regulator (ECP) until the maximum indentation depth is reached (3mm). During the process, variation of both the indentation depth and the air pressure inside the probe was monitored. The experiment was conducted at four different locations for each silicon sample and at each location the same test was repeated three times. After each test, the pressure variation inside the probe was used to compute the indentation force. Fig. 11 (a) shows the variation of the computed indentation force with the indenter displacement for two different test locations in each simulated tissue sample. Elastic modulus at each test point was computed using (6), (7) and (8). Thickens of the tissue sample was 20mm ($^{d}/_{r} = 5$). The results are given in Fig. 11 (b). It is clear from Fig. 11 (b) that both (7) and (8) gives very similar estimates for elastic modulus while (6) overestimates it. Average stiffness of the two tissue samples estimated using (7) were 25±5KPa and 10.±4KPa.

Further, in order to verify the ability of the probe to measure tissue stiffness while moving over the tissue surface, a series of tests were carried out on a simulated silicon phantom containing four embedded tumors. The silicon phantom has a square base and a convex upper surface profile. The profile height varied along the y-axis of the tissue: the thickness is 4 mm at the center and it reduces to 2 mm towards the edges. Stiffness of the silicone phantom was 26.4KPa and tumors were up to six times stiffer than the surrounding tissue. Tumors were embedded 2mm below the tissue surface. Size and the tumor-tissue stiffness ratio for each tumor are given in Fig. 12. During the indentation test, the probe is held vertically and the scanning was performed horizontally (i.e. parallel to the y-axis) with aid of a robotic manipulator (Fanuc M6iB). The robot paths were deliberately chosen to not follow the curved surface of the phantom in order to effectively explore the sensor skill on coping with irregular surfaces. Results are shown in Fig. 12. It is clear from Fig. 12 that the probe produces a fairly constant stiffness map for the healthy area of the tissue and it has not respond to the tissue curvature. Tumors are indicated as high stiffness regions and all the four tumors are clearly visible on the map. Hence this probe can be used to identify the presence and location of the tumors through the generation of a tissue stiffness map even for non-planer tissue profiles. However, tumors on the stiffness map become less clear as tumor-tissue stiffness ratio decreases and tumor size decreases.

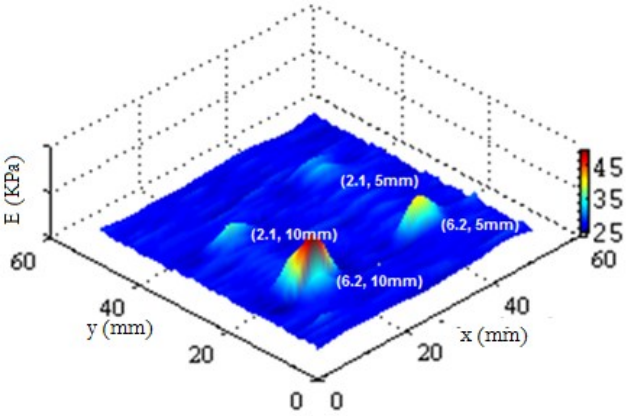

Fig. 12. the stiffness map for the silicone phantom with curved upper surface.

V. Conclusion

A novel technique for estimating the stiffness distribution of soft tissues using an air-float stiffness probe have been described and discussed. The probe employs an indentation depth sensing mechanism that can be used to estimate absolute indentation depth. Hence the probe has the ability to estimate tissue stiffness in non-planner tissue profiles. Verification tests carried out on simulated silicon samples

showed that the probe is capable of estimating tissue stiffness values with high accuracy and repeatability. This probe is unique in its ability to have an adjustable force range which is useful in limiting the forces applied onto the soft tissue thus avoiding accidental tissue damages. Indentation force can be adjusted through the control and regulation of the air pressure inside the probe. However, this makes pressure regulation and control essential for the correct operation of the probe. Further work aims at improving the sensor fabrication quality and modeling the sensor behavior under variety of operating conditions. Specially, modeling the behavior of the sensor under dynamic conditions, using moving mesh methods in FEA techniques is being done. Further, we aim to carry out ex-vivo and in-vivo trials to evaluate the sensors potential as a stiffness probe to detect tissue abnormalities.

REFERENCES

[1] T. A. Krouskop, T. M. Wheeler, F. Kallel, B. S. Garra, and T. Hall, "Elastic moduli of breast and prostate tissues under compression," Ultrason. Imag., vol. 20, no. 4, pp. 260–274, 1998.

[2] D.O.Uribe, R.Stroop, T.Hemsel, and J.Wallaschek ,"Development of a biomedical tissue differentiation system using piezoelectric actuators,"IEEE International Frequency Control Symposium, pp. 91 – 94, 2008

[3] H. Liu, J. Li, X. Song, L.D. Seneviratne, and K. Althoefer, "Rolling indentation probe for tissue abnormality identification during minimally invasive surgery," IEEE Transactions on Robotics, vol. 27, pp. 450-460, 2011

[4] K. Althoefer, D. Zbyszewski, H. Liu, P. Puangmali, L.D. Seneviratne, B. Challacombe, and D. Murphy, "Air-cushion force sensitive probe for soft tissue investigation during minimally invasive surgery," IEEE Sensors, pp.827-830, 2008

[5] I.B. Wanninayake, P. Dasgupta, L.D. Seneviratne, and K. Althoefer, 'Air-float Palpation Probe for Tissue Abnormality Identification During Minimally Invasive Surgery' IEEE Transactions on Biomedical Engineering, vol 60, no. 10, pp. 2735-2744, 2013

[6] K. Sangpradit, H. Liu, P. Dasgupta, K. Althoefer, and L.D. Seneviratne, "Finite-element modeling of soft tissue rolling indentation.," IEEE Transactions on Biomedical Engineering, vol. 58, pp. 3319-3327, 2012

[7] K. Sangpradit, H. Liu, P. Dasgupta, L.D. Seneviratne, and K. Althoefer, "Tissue identification using inverse finite element analysis of rolling indentation." IEEE International Conference on In Robotics and Automation, pp. 1250-1255, 2009

[8] I.B. Wanninayake, K. Althoefer, and L.D. Seneviratne, "Novel Air-float Tactile Array for Stiffness Characterization in Soft Tissue Palpation," Procedia Engineering, Volume 41, pp. 281-288, 2012

[9] A. M. Sabatini, P. Dario, and M. Bergamasco, "Interpretation of mechanical properties of soft tissues from tactile measurements," Exp. Robot., vol. 139, pp. 152–162, 1990.

[10] J. Dargahi, S. Najarian, V. Mirjalili, and B. Liu, "Modeling and testing of a sensor capable of determining the stiffness of biological tissues," Can. J. Electr. Comput. Eng., vol. 32, no. 1, pp. 45–51, 2007.

[11] M.P. Ottensmeyer and J.K. Salisbury, "In Vivo Data Acquisition Instrument for Solid Organ Mechanical Property Measurement", In Proceedings of the 4th International Conference on Medical Image Computing and Computer-Assisted Intervention (MICCAI '01), Wiro J. Niessen and Max A. Viergever (Eds.). Springer-Verlag, London, UK, UK, 975-982.

[12] K. L. Johnson, Contact Mechanics. Cambridge, U.K. Cambridge Univ. Press, 1985.

[13] P. Fong, "Sensing, acquisition, and interactive playback of data-based models for elastic deformable objects," the International Journal of Robotics Research, vol. 28, no. 5, pp. 630–655, May 2009.

[14] B. Frank, R Schmedding, c. Stachniss, m. Teschner, and w. Burgard, "Learning the elasticity parameters of deformable objects with a manipulation robot," pp. 1877–1883, oct. 2010.

[15] J. Lang, D. K. Pai, and R. J. Woodham, "Acquisition of elastic models for interactive simulation," the International Journal of Robotics Research, vol. 21, no. 8, pp. 713–733, Aug. 2002.

[16] I.B. Wanninayake, L.D. Seneviratne, K. Althoefer, "Novel indentation depth measuring system for stiffness characterization in soft tissue palpation", in Proc. IEEE Int. Conf. Robot. Automation, 2012, 4648-4653

[17] D.C. Lin, D.I. Shreiber, E.K. Dimitriadis, and F. Horkay,"Spherical indentation of soft matter beyond the Hertzian regime: numerical and experimental validation of hyperelastic models", Biomechanics and Modeling in Mechanobiology,8,345-358, 2009

[18] H. Liu, J. Li, Q. Poon, L.D. seneviratne, and K. Althoefer, "Miniaturized force-indentation depth sensor for tissue abnormality identifaction during laparoscopic surgery", IEEE international conference on Robotics and Automation, pp 3654-3659, 2010

[19] C. Anthony, Fischer-Cripps, "Introduction to Contact Mechanics", 2nd ed., New York, NY: Springer, 2007, ch. 6, pp. 101–114.

[20] Bo. Qiang, J. Greenleaf, M. Oyen, and X. Zhang, "Estimating material elasticity by spherical indentation load-relaxation tests on viscoelastic samples of finite thickness," *IEEE Transactions on Ultrasonics, Ferroelectrics and Frequency Control,* , vol.58, no.7, pp.1418-1429, July 2011

[21] E. K. Dimitriadis, F. Horkay, J. Maresca, B. Kachar, and R. S. Chadwick, "Determination of elastic moduli of thin layers of soft material using the atomic force microscope," Biophys. J., vol. 82, pp.2798–2810, May 2002.